Determination of the reflectivity of crystals by ptychography

Cite as: AIP Advances 12, 125219 (2022); doi: 10.1063/5.0102867
Submitted: 11 July 2022 • Accepted: 28 November 2022 •
Published Online: 15 December 2022

View Online

Export Citation

CrossMark

Kai S. Schulze[a)]

AFFILIATIONS

Helmholtz-Institut Jena, 07743 Jena, Germany; Friedrich-Schiller-Universität Jena, 07743 Jena, Germany; and GSI Helmholtzzentrum für Schwerionenforschung, 64291 Darmstadt, Germany

[a)]Author to whom correspondence should be addressed: kai.sven.schulze@uni-jena.de

ABSTRACT

The x-ray reflectivity of crystals is an important measure for their quality. Its knowledge is of interest for the development of materials as well as for the design of x-ray optical instruments, while the determination of the reflectivity curve is not trivial. This article presents an approach to retrieve the reflectivity curve of crystals based on ptychography. The method is demonstrated on the examples of silicon and diamond of which the reconstructed reflectivity curves agree well with theoretical expectations. Thus, this method offers promising perspectives in the detection of small crystalline defects and in the design of future instruments for x rays.

© 2022 Author(s). All article content, except where otherwise noted, is licensed under a Creative Commons Attribution (CC BY) license (http://creativecommons.org/licenses/by/4.0/). https://doi.org/10.1063/5.0102867

Crystals are indispensable in x-ray optics. They find application as monochromators,[1–4] spectrometers,[5–7] polarizers,[8–12] focusing elements,[13,14] or simply, reflectors. The common concept of these applications is diffraction at the periodic crystalline structure which, in turn, occurs only in a very narrow angle and wavelength range. The knowledge of the intrinsic reflectivity curve of a crystal, which means the reflectivity that is expected for an incident monochromatic plane wave in dependence on the angle of incidence, is of importance for the design of x-ray optical instruments. In particular, the peak reflectivity and its angular width are critical properties. They are, for example, decisive for the design of monochromators and very topical for the development of cavity mirrors for x-ray free electron laser oscillators.[15]

The reflectivity curve of crystals also has significance for the precise determination of x-ray wavelengths and lattice parameters. Both can be traced directly back to the Système International definition of meter via comparison with reference crystals.[16] The asymmetric shape of the reflectivity curves leads to a small angular shift of the signal. Currently, the necessary corrections are estimated based on the dynamical theory of x-ray diffraction.[16]

Also, for other instruments or experiments, the reflectivity is usually estimated based on the dynamical theory of x-ray diffraction,[17] since its measurement is not trivial. The measured curves are always broadened by the apparatus function. Accordingly, different approaches were used to minimize this broadening in the past. Using crystals with different asymmetric Bragg reflections in front of the sample is the most common technique to minimize the apparatus function.[18,19] For broad reflectivity curves, for example in back-reflection geometry,[15] the divergence of a synchrotron beam might even be narrow enough.

The measurement of the reflectivity curve also gives information about the structural quality of a crystal. Whereas dislocations can be determined even with large apparatus functions, small strains might only be visible by a detailed comparison with theoretical expectations of the reflectivity curve.[19]

Blurring of small structures by the apparatus function is also well known in imaging. A powerful technique to improve the resolution in imaging is ptychography.[20] In the x-ray range, structures in the sub-10 nm range have recently been observed with the help of ptychography.[21,22] Combined with Bragg diffraction, the strain fields in crystals can be mapped with a high resolution (the so-called Bragg ptychography).[23] However, this method is not only limited to imaging. In principle, every measurement that delivers an interference pattern of two distributions could be improved by ptychography. A recent example is the temporal measurement of attosecond laser pulses.[24]

Here, I show theoretically and experimentally how the reflectivity curve can be obtained with the help of only two crystals using

ptychography. The method is demonstrated on crystals that are of importance for modern x-ray optical instruments: silicon and diamond.

The essential idea is a double-crystal diffractometer consisting of the sample crystal and a thick crystal in von-Laue geometry as sketched in Fig. 1(a). In a double-crystal configuration, x rays are successively reflected at the two crystals. If both crystals and their Bragg reflections are identical (non-dispersive arrangement) and aligned to fulfill the Bragg condition, the measured intensity, when one of the crystals is rocked, will be the convolution of the plane-wave reflectivity of both crystals.[17] However, this is only the case if the divergence of the beam before the setup is larger than the angular width of the plane-wave reflectivity of the first crystal.

The second crystal in von-Laue geometry, where the diffracted beam exits the crystal at the rear surface, gives additional information, enabling the deconvolution of the two plane-wave reflectivity curves. Assuming a spatially narrow x-ray beam, the paths of the incident and the diffracted beam span a triangle inside the crystal. This triangle with its base length $2l$ is known as the Borrmann fan. The spatial distribution of the field amplitude $D_h(x')$ of the diffracted beam along the base of the Borrmann fan depends on the distribution $D_f(x)$ on the front side as[25]

$$D_h(x') = A\int_{-l}^{l} D_f(x-x')J_0\left(B\sqrt{l^2-x^2}\right)dx. \tag{1}$$

Here, J_0 is the Bessel function of zeroth order and A and B are constants that depend on wavelength, crystal, and Bragg reflection.[25] Thus, the spatial field distribution at the rear side of the second crystal can be used to gain information about the field at the front side. However, how is $D_f(x)$ connected to the reflectivity of the first crystal?

In a double-crystal configuration, $D_f(x)$ is the far-field diffraction pattern caused by the angle dependent reflectivity $r_1(\Delta\Theta)$. If we describe the diffracted field by the first crystal by an infinite sum of plane waves,

$$D_1(\vec{r}) = \iiint_{|\vec{K}|=k} D_1(\vec{K})\exp\left(-2\pi i\vec{K}\cdot\vec{r}\right)dK_x dK_y dK_z, \tag{2}$$

we see how the spatially dependent amplitude $D_1(\vec{r})$ depends on the angular one $D_1(\vec{K})$. If one separates a central wave that fulfills the Bragg condition of the second crystal, the wave $D_1(\vec{r})$ becomes

$$D_1(\vec{r}) = \iiint_{|\vec{K}|=k} D_1(\vec{K})\exp\left[-2\pi i(\vec{K}-\vec{k}_0)\cdot\vec{r}\right]dK_x dK_y dK_z \cdot\exp\left(-2\pi i\vec{k}_0\cdot\vec{r}\right). \tag{3}$$

The vector $\vec{K}-\vec{k}_0$ describes the deviation from the Bragg condition. Its projection on the surface of the second crystal is consequently

$$(\vec{K}-\vec{k}_0)\cdot\vec{r}_{\mathrm{surf}} = \gamma_0 k\Delta\Theta x, \tag{4}$$

and the field distribution on the surface of the second crystal becomes

$$D_f(x) = \int_{-\infty}^{\infty} D_1(\Delta\Theta)\exp(-2\pi i\gamma_0 k\Delta\Theta x)\,d\Delta\Theta. \tag{5}$$

Here, $\Delta\Theta$ is the angular coordinate, while k is the wave number and γ_0 is the cosine of the angle between the beam and the surface of

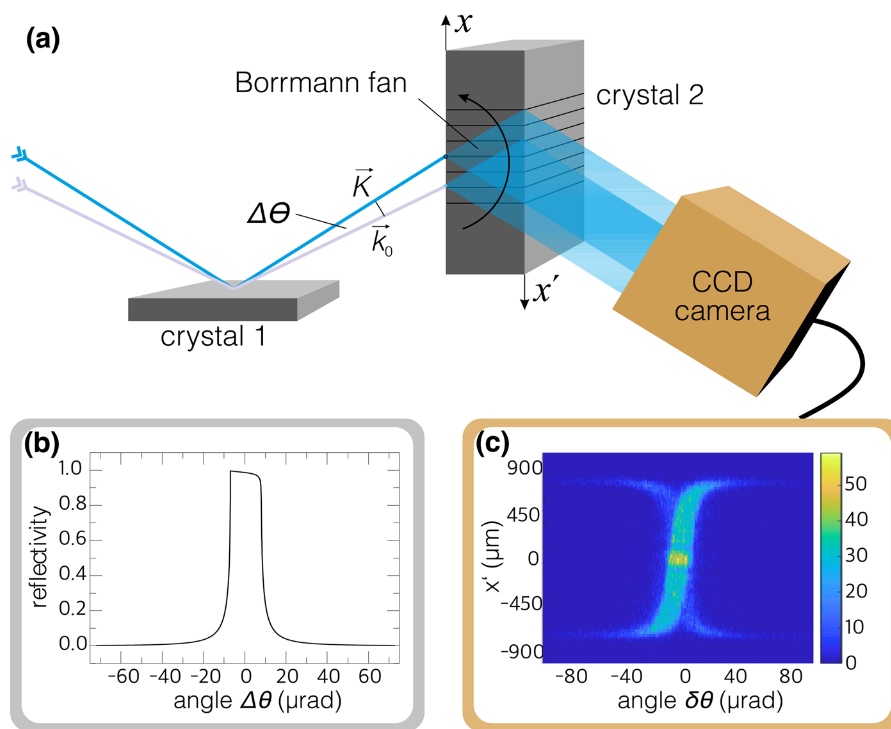

FIG. 1. (a) The reflectivity curve of crystal 1, the sample object, is obtained using a second crystal, which acts as an angular filter via its own reflectivity curve and as a Fourier transformer. Crystal 2 is used in a special case of the so-called von-Laue geometry, where the lattice planes (black lines) are perpendicular to the front and rear surface. (b) The theoretical reflectivity curve of a diamond crystal at the 400 lattice planes. (c) The spatial distribution of the photon number acquired during the experiment for different angles of crystal 2 in relation to crystal 1 for the 400 Bragg reflection at diamond. Of these data, the plane-wave reflectivity of crystal 1 can be obtained via a ptychographic approach without any assumptions on its shape.

© Author(s) 2022

the second crystal. Especially in x-ray tubes, the divergence of the source is much broader than the angular width of the crystal reflectivity. Therefore, we can assume that the incident field amplitude D_0 is constant, and thus, D_1 just depends on the angle-dependent reflectivity of the crystal,

$$D_1(\Delta\Theta) = D_0 r_1(\Delta\Theta). \tag{6}$$

It follows that

$$D_f(x) = D_0 \int_{-\infty}^{\infty} r_1(\Delta\Theta) \exp(-2\pi i \gamma_0 k \Delta\Theta x)\, d\Delta\Theta. \tag{7}$$

Substituting Eq. (7) in (1) and changing the order of integration give the field distribution at the rear surface of the second crystal,

$$D_h(x') = D_0 A \int_{-\infty}^{\infty} r_1(\Delta\Theta) \exp\big(2\pi i \gamma_0 k \Delta\Theta x'\big) \cdot \underbrace{\int_{-l}^{l} \exp(-2\pi i \gamma_0 k \Delta\Theta x) J_0\big(B\sqrt{l^2 - x^2}\big)\, dx}_{r_2(\Delta\Theta)}\, d\Delta\Theta. \tag{8}$$

The term above the underbrace can be identified as the plane wave reflectivity of the second crystal.[25] Therefore, the field distribution at the rear surface is the inverse Fourier transform of the product of the angle-dependent plane-wave reflectivities of both crystals,

$$D_h(x') = A' \mathcal{F}^{-1}[r_1(\Delta T) r_2(\Delta T)], \tag{9}$$

with $\Delta T = \gamma_0 k \Delta\Theta$ being the variable for the Fourier transformation. One can regard r_1 as the object and r_2 as the probe. By rocking the second crystal, the probe, the angular relation changes, and, thus, the field distribution at the rear surface,

$$D_h(x', \delta T) = A' \mathcal{F}^{-1}[r_1(\Delta T) r_2(\Delta T - \delta T)]. \tag{10}$$

Integration of the square of the absolute value of $D_h(x', \delta T)$ over the base of the Borrmann fan gives the convolution,

$$|D_h(\delta T)|^2 = A'^2 \big(|r_1(\Delta T)|^2 * |r_2(-\Delta T)|^2\big)(\delta T). \tag{11}$$

This convolution is the usual result of double-crystal diffraction experiments.[17]

Equation (10) is the typical expression used in the extended ptychographic iterative engine. This algorithm searches iteratively for two functions, $r_1(\Delta T)$ and $r_2(\Delta T)$, that minimize the difference between the measured amplitude $\sqrt{I(x', \delta T)}$ and the calculated one $D_h(x', \delta T)$,

$$\min_{r_1(\Delta T), r_2(\Delta T)} \sum_{\delta T} \sum_{x'} \times \Big| \sqrt{I(x', \delta T)} - \big|A' \mathcal{F}^{-1}[r_1(\Delta T) r_2(\Delta T - \delta T)]\big| \Big|^2. \tag{12}$$

By measuring the field distribution at the base of the Borrmann fan for different angular relations of the crystals, the ptychography algorithm can determine the two angular dependent reflectivities. Since $D_h(x')$ is sensitive on the actual crystalline structure—a fact that found application in section topography—the second crystal must have a nearly perfect or uniformly disturbed structure to obtain reasonable results.

At each iteration in the algorithm, the functions of the object and the probe are updated using respective update functions. The following update functions, which enable a fast convergence, were used:

$$U_O = c_1 \frac{r_2(\Delta T - \delta T)^*}{\max(|r_2(\Delta T - \delta T)|^2)} (\Phi - \Psi), \quad U_P = c_2 \frac{r_1(\Delta T - \delta T)^*}{\max(|r_1(\Delta T - \delta T)|^2)} (\Phi - \Psi), \tag{13}$$

with

$$\Phi = \mathcal{F}\Big\{\sqrt{I(x', \delta T)} \exp\big[i \arg\big(\mathcal{F}^{-1}(\Psi)\big)\big]\Big\} \tag{14}$$

and

$$\Psi = r_1(\Delta T) r_2(\Delta T - \delta T). \tag{15}$$

A reliable convergence was obtained with $c_1 = 1$ and $c_2 = 0.15$.

For the experimental demonstration, I used two pairs of crystals: a pair of silicon crystals and a pair of high-temperature high-pressure diamonds. The first silicon crystal had a polished ⟨110⟩ surface, while the second was a 1.3 mm-thick crystal with a ⟨001⟩ surface. Both crystals were aligned to the 220 Bragg reflection. Thus, the second crystal was used in von-Laue geometry. This crystal also acted as a polarization filter[26] to determine the reflectivity perpendicular to the plane of diffraction (σ component). In the case of diamond, both crystals were 0.5 mm thick with a ⟨100⟩ surface. While the first diamond was aligned to the symmetric 400 Bragg reflection, the second one was aligned to the 004 one. In contrast to silicon, the polarization component in the plane of diffraction (π component) is not suppressed by the rather thin second diamond crystal. Since an unpolarized source was used in this experiment, a germanium crystal supporting the 333 Bragg reflection with a Bragg angle of 45.03° was introduced upstream the diamonds to act as a polarizer.

The experiment, as sketched in Fig. 1(a), was carried out at a rotating anode x-ray source (RIGAKU). The copper K_α radiation was collimated by a multilayer optic in order to get an almost parallel beam with a divergence of about 0.4 mrad. The intensity distribution at the rear of the respective second crystal was acquired by a Princeton Instruments CCD camera having a 13.5 μm pixel size. Since the intensity distribution is broadened by the horizontal beam size, 70 μm-thick and 40 μm-thick slits were used in front of the setup for silicon and diamond, respectively. In the case of diamond, the intensity distribution along the Borrmann fan dependent on the angular deviation is shown in Fig. 1(c). The second crystal was scanned with a step width of 1.1 μrad. Together with an acquisition time of 50 s per step, one measurement took about 2 h. In order to prevent thermal drifts during this time, the temperature was stabilized with an accuracy of a few 0.1 K.

The algorithm to solve Eq. (12) and to get the reflectivity curves out of the measured intensity distribution was implemented in MATLAB. As an initial guess, $r_1(\Delta T)$ was set constant, while $r_2(\Delta T)$ was set to the theoretical curve in order to achieve a fast and reliable convergence. The number of iterations was fixed to 500. However,

© Author(s) 2022

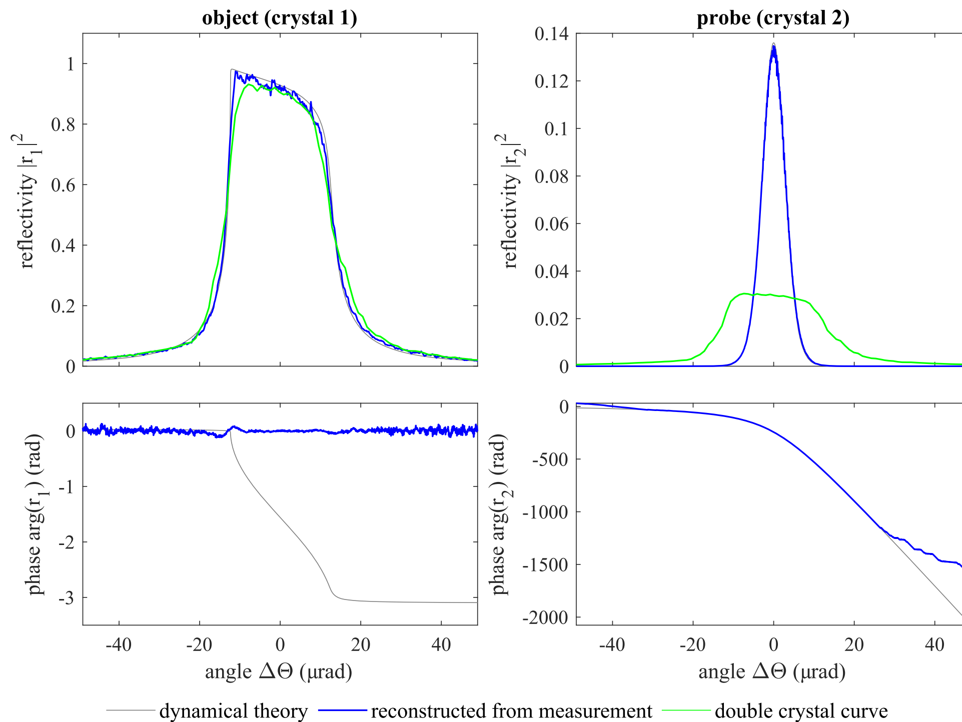

FIG. 2. Reflectivity of the silicon 220 Bragg reflection for the symmetric Bragg (left) and von-Laue (right) cases retrieved via ptychography. Apart from the oscillation close to the sharp edge of the reflectivity curve of crystal 1, the results meet the theoretical predictions by the dynamical theory of x-ray diffraction. The phase of the reflectivity of crystal 1 could not be reconstructed, because of its small variation in comparison with crystal 2. The results are compared with the curve obtained by double-crystal diffraction.

even after just a few iterations, $r_1(\Delta T)$ already shows the characteristic shape of the reflectivity. To compare the retrieved reflectivity curves with theoretical predictions, the integral of the curves is normalized to the integral retrieved by conventional double-crystal diffraction measurements.

Figures 2 and 3 show the results of this reconstruction for silicon 220 and diamond 400, respectively. In addition, the curves are compared with the reflectivity curves calculated based on the dynamical theory of x-ray diffraction. The amplitudes of the retrieved reflectivities are well described by the theoretical

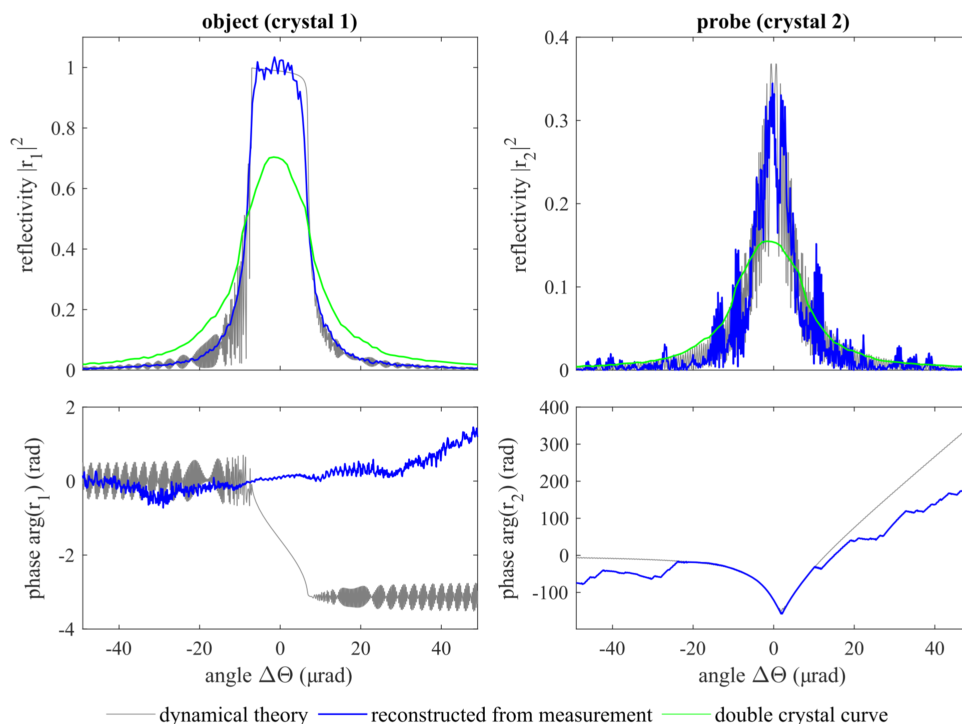

FIG. 3. Reflectivity of the diamond 400 Bragg reflection for the symmetric Bragg (left) and von-Laue (right) cases retrieved via ptychography. Both crystals were 500 μm-thick high-temperature high-pressure diamonds with an almost perfect crystalline structure as revealed by the good agreement between the retrieved and theoretical reflectivity curves. Also, in this case, the phase of the reflectivity of crystal 1 could not be reconstructed.

© Author(s) 2022

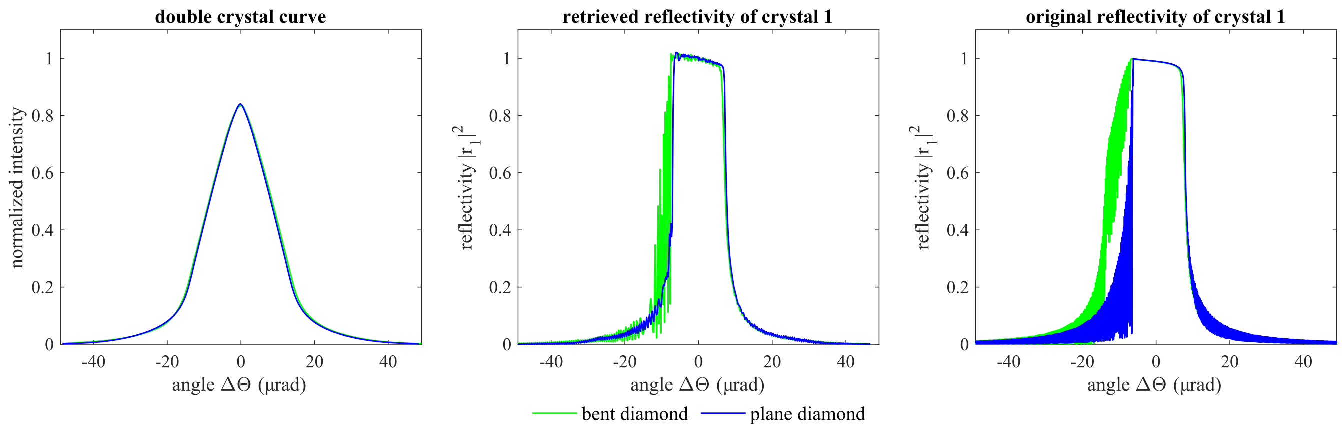

FIG. 4. Simulation of the influence of crystal bending on the double-crystal curve and the reflectivity curve for 500 μm-thick diamonds and the 400 Bragg reflection. Whereas the change in the double-crystal curve is barely noticeable, the retrieved reflectivity curve of a bent diamond with 10 m bending radius shows the typical oscillations on the left side of the curve and reproduce well the original reflectivity used for the simulation.

expectations. However, since the phase of r_2 varies by several π, the expected phase variation of r_1 of π could not be reconstructed. In addition, the measured intensity distribution is the sum over different positions on the crystal. The variations in the thickness and crystalline quality also hinder the reconstruction of the phase. The missing phase information leads to small artifacts in the amplitude at the sharp edge in front of the reflectivity curve. The comparison of the reflectivity curves with the double-crystal rocking curves obtained by the same setup clearly shows the improvement in the angular resolution, in particular for diamond.

The increased resolution offered by this ptychographic approach can reveal small changes in the reflectivity curve caused by the strain inside the crystal, for instance. To demonstrate this capability, I simulated the expected intensity distribution at the base of the Borrmann fan for two double crystal experiments and used the previously described algorithm to retrieve the reflectivity curves: (i) for two flat diamond crystals, similar to the real experiment shown in Fig. 3, and (ii) a diamond crystal bent in the diffraction plane as a first crystal. The bending causes a strain perpendicular to the surface of the crystal, which consequently changes the reflectivity curve. This strain is well-defined by the bending radius of the crystal, and its influence on the reflectivity curve can be calculated within the dynamical theory of x-ray diffraction, for instance by using the Takagi–Taupin formalism.[17] This allows us to test the sensitivity of the presented ptychographic approach with well-defined, small strain fields.

A large bending radius of 10 m, for instance, causes only a slight change in the reflectivity curve. Using a conventional double-crystal setup, this change is barely visible as shown in Fig. 4. In strong contrast, the retrieved reflectivity curves clearly show the influence of bending. The fringes on the left side of the curve of the bent crystal are intensity oscillations caused by the interference of waves diffracted at different positions inside the crystal. Their period is in the order of 0.1 μrad, showing the high angular resolution that is possible with this method. However, the oscillations are not reproduced in detail compared to the original reflectivity because of the finite pixel size and, thus, the limited resolution of the required camera.

If one considers experimental uncertainties such as limited photon numbers and angle uncertainties, even a larger strain will not be noticeable in the double crystal curve. In contrast, ptychography is quite robust against such experimental uncertainties so that, even in non-ideal setups, small changes in the reflectivity of crystals become detectable.

In conclusion, the determination of the reflectivity curve of crystals shows that ptychography is not only a valuable tool in imaging, in particular with x rays, but can also be applied to other applications. The retrieved reflectivities of silicon and diamond fit well to the expectations by the dynamical theory of x-ray diffraction for (nearly) perfect crystals. Particularly interesting are the results for diamond. The high-temperature high-pressure diamonds used here have distinct regions with an almost perfect crystalline structure which, in turn, implies a peak reflectivity close to 100% for the 400 reflection and copper K_α radiation. This is even more impressive if one considers the sensitivity of the reflectivity curve to a small strain, as demonstrated by the simulation. The experimental results presented here contain a high amount of noise because of the low count rate on each pixel of the camera. Transferring this technique to synchrotrons would considerably improve the results and would make different Bragg angles accessible. Since the synchrotrons enable the illumination of small areas, phase retrieval might also be possible. Furthermore, computational optimization methods known from ptychographic imaging, such as position correction[27] and multi-state ptychography,[28] can be applied to the data obtained in non-ideal environments to get the best results for the reliable study of the reflectivity of crystals.

This work was funded by the Deutsche Forschungsgemeinschaft (DFG) under Grant Nos. 416700351 and 392856280 within the Research Unit FOR2783. I am indebted to R. Lötzsch, H. Bernhardt, I. Uschmann, R. Röhlsberger, and G. G. Paulus for fruitful discussions and their valuable comments on the manuscript.

© Author(s) 2022

AUTHOR DECLARATIONS

Conflict of Interest

The author has no conflicts to disclose.

Author Contributions

Kai S. Schulze: Conceptualization (equal); Formal analysis (equal); Funding acquisition (equal); Methodology (equal); Writing – original draft (equal).

DATA AVAILABILITY

The data that support the findings of this study are available from the corresponding author upon reasonable request.

REFERENCES

[1] R. Caciuffo, S. Melone, F. Rustichelli, and A. Boeuf, "Monochromators for x-ray synchrotron radiation," Phys. Rep. **152**, 1–71 (1987).

[2] R. Verbeni, F. Sette, M. H. Krisch, U. Bergmann, B. Gorges, C. Halcoussis, K. Martel, C. Masciovecchio, J. F. Ribois, G. Ruocco, and H. Sinn, "X-ray monochromator with 2×10^8 energy resolution," J. Synchrotron Radiat. **3**, 62–64 (1996).

[3] T. Ishikawa, K. Tamasaku, and M. Yabashi, "High-resolution X-ray monochromators," Nucl. Instrum. Methods Phys. Res., Sect. A **547**, 42–49 (2005).

[4] A. I. Chumakov, I. Sergeev, J.-P. Celse, R. Rüffer, M. Lesourd, L. Zhang, and M. Sánchez del Río, "Performance of a silicon monochromator under high heat load," J. Synchrotron Radiat. **21**, 315–324 (2014).

[5] J. Hoszowska, J.-C. Dousse, J. Kern, and C. Rhême, "High-resolution von Hamos crystal x-ray spectrometer," Nucl. Instrum. Methods Phys. Res., Sect. A **376**, 129–138 (1996).

[6] G. Hölzer, M. Fritsch, M. Deutsch, J. Härtwig, and E. Förster, "$K\alpha_{1,2}$ and $K\beta_{1,3}$ x-ray emission lines of the $3d$ transition metals," Phys. Rev. A **56**, 4554 (1997).

[7] U. Zastrau, L. B. Fletcher, E. Förster, E. C. Galtier, E. Gamboa, S. H. Glenzer, P. Heimann, H. Marschner, B. Nagler, A. Schropp, O. Wehrhan, and H. J. Lee, "Bent crystal spectrometer for both frequency and wavenumber resolved x-ray scattering at a seeded free-electron laser," Rev. Sci. Instrum. **85**, 093106 (2014).

[8] H. Cole, F. W. Chambers, and C. G. Wood, "X-ray polarizer," J. Appl. Phys. **32**, 1942 (1961).

[9] M. Hart, D. P. Siddons, Y. Amemiya, and V. Stojanoff, "Tunable x-ray polarimeters for synchrotron radiation sources," Rev. Sci. Instrum. **62**, 2540–2544 (1991).

[10] Y. Hasegawa, Y. Ueji, K. Okitsu, J. M. Ablett, D. P. Siddons, and Y. Amemiya, "Transmission-type x-ray linear polarizer with perfect crystals," J. Synchrotron Radiat. **5**, 738 (1998).

[11] E. E. Alp, W. Sturhahn, and T. S. Toellner, "Polarizer-analyzer optics," Hyperfine Interact. **125**, 45 (2000).

[12] B. Marx, K. S. Schulze, I. Uschmann, T. Kämpfer, R. Lötzsch, O. Wehrhan, W. Wagner, C. Detlefs, T. Roth, J. Härtwig, E. Förster, T. Stöhlker, and G. G. Paulus, "High-precision x-ray polarimetry," Phys. Rev. Lett. **110**, 254801 (2013).

[13] C. J. Sparks, Jr., G. E. Ice, J. Wong, and B. W. Batterman, "Sagittal focusing of synchrotron x-radiation with curved crystals," Nucl. Instrum. Methods Phys. Res. **195**, 73–78 (1982).

[14] Z. Wenli, J. Xiaoming, W. Jiayang, J. Yuhui, and L. Gongchun, "Studies on focusing performances of the bent crystal monochromator," Chin. Phys. C **19**, 858–864 (1995).

[15] Y. Shvyd'Ko, S. Stoupin, V. Blank, and S. Terentyev, "Near-100% Bragg reflectivity of X-rays," Nat. Photonics **5**, 539 (2011).

[16] M. H. Mendenhall, A. Henins, L. T. Hudson, C. I. Szabo, D. Windover, and J. P. Cline, "High-precision measurement of the x-ray Cu $K\alpha$ spectrum," J. Phys. B: At., Mol. Opt. Phys. **50**, 115004 (2017).

[17] A. Authier, *Dynamical Theory of X-Ray Diffraction* (Oxford University Press, New York, 2001), Vol. 11.

[18] R. Bubáková, "The diffraction pattern of Ge (111)—Asymmetrical Bragg case," Cechoslovackij fiziceskij zurnal B **12**, 776–783 (1962).

[19] F. Masiello, G. Cembali, A. I. Chumakov, S. H. Connell, C. Ferrero, J. Härtwig, I. Sergeev, and P. Van Vaerenbergh, "Rocking curve measurements revisited," J. Appl. Crystallogr. **47**, 1304–1314 (2014).

[20] A. M. Maiden, M. J. Humphry, F. Zhang, and J. M. Rodenburg, "Superresolution imaging via ptychography," J. Opt. Soc. Am. A **28**, 604–612 (2011).

[21] A. Schropp, R. Hoppe, J. Patommel, D. Samberg, F. Seiboth, S. Stephan, G. Wellenreuther, G. Falkenberg, and C. G. Schroer, "Hard x-ray scanning microscopy with coherent radiation: Beyond the resolution of conventional x-ray microscopes," Appl. Phys. Lett. **100**, 253112 (2012).

[22] F. Pfeiffer, "X-ray ptychography," Nat. Photonics **12**, 9 (2018).

[23] S. O. Hruszkewycz, M. Allain, M. V. Holt, C. E. Murray, J. R. Holt, P. H. Fuoss, and V. Chamard, "High-resolution three-dimensional structural microscopy by single-angle Bragg ptychography," Nat. Mater. **16**, 244 (2017).

[24] M. Lucchini, M. H. Brügmann, A. Ludwig, L. Gallmann, U. Keller, and T. Feurer, "Ptychographic reconstruction of attosecond pulses," Opt. Express **23**, 29502–29513 (2015).

[25] D. Simon and A. Authier, "Application de la théorie dynamique de S. Takagi au contraste d'un défaut plan en topographie par rayons X. II. Franges de moiré," Acta Crystallogr., Sect. A: Cryst. Phys., Diffr., Theor. Gen. Crystallogr. **24**, 527–534 (1968).

[26] K. S. Schulze, B. Marx, I. Uschmann, E. Förster, T. Stöhlker, and G. G. Paulus, "Determination of the polarization state of x rays with the help of anomalous transmission," Appl. Phys. Lett. **104**, 151110 (2014).

[27] A. M. Maiden, M. J. Humphry, M. C. Sarahan, B. Kraus, and J. M. Rodenburg, "An annealing algorithm to correct positioning errors in ptychography," Ultramicroscopy **120**, 64–72 (2012).

[28] P. Thibault and A. Menzel, "Reconstructing state mixtures from diffraction measurements," Nature **494**, 68–71 (2013).

© Author(s) 2022